Signal-to-noise Ratio Estimation for SEM Single Image using Cubic Spline Interpolation with Linear Least Square Regression

K. S. Sim, *Member, IAENG*, F. F. Ting, *Member, IAENG*, J. W. Leong, and C. P. Tso

***Abstract*— A novel technique based on cubic spline interpolation with linear least square regression (CSILLSR) is developed to calculate the signal-to-noise ratio (SNR) of scanning electron microscope (SEM) images. The SNR from CSILLSR method is compared with methods of nearest, linear interpolation, a combination of linear interpolation and nearest, non-linear least square regression, autocorrelation Levinson-Durbin recursion, and adaptive slope nearest neighbourhood. Samples of SEM images with various accelerating voltages, beam diameters, surface tilts and contrast were applied to evaluate the performance of CSILLSR method in terms of SNR values of the SEM images. The new method is able to generate more accuracy results than the other six methods. In addition, the CSILLSR Wiener filter appears to be the best filter to reduce and remove white Gaussian noise from SEM images as compared to the average filter and median filter.**

***Index Terms*— Gaussian noise, Cubic Spline Interpolation, Linear Least Square Regression, SNR estimation**

I. Introduction

THE quality of grayscale images and scanning electron microscope (SEM) images is always degraded by noise [1]. The SNR parameter plays a crucial role to determine the quality of SEM image. In semiconductor and medical industry, the loss of important image information needs to be avoided.

In the past, SNR estimation techniques for SEM images had been introduced. Reference [2] had developed cross-correlation function (CCF) using the Fourier transforms. Then, CCF technique was unable to compute the SNR measurement for both stored and extant images. Reference [3] also applied the similar CCF in digital image averaging. The application of CCF is extended to compute the resolution values of SEM critical dimension [4]. To implement the cross-correlation function, the alignment between the two images must be performed properly, making this application difficult.

II. Literature Review

In order to solve the mentioned drawback, [5] set up an approach that can allow SNR estimation to be measured by using a single image. In this method, a white noise source is introduced to the image. Then, two techniques are proposed for single image SNR computation. These two techniques are named as nearest method and linear interpolation [6]. However, these two techniques obtain poor accuracy, which may be due to the characteristics of the images. It can be due to images with different texture, magnification, aperture size, and resolution, which can influence the SNR accuracy. Hence, in [7] the autoregressive (AR) model interpolation is applied to compute the SNR of the noisy image. However, the precision of the AR model is also affected and bounded by the nature of the images.

Then the AR method is improved by combining with the Lagrange time delay (LTD) estimator [8]. This algorithm is termed as Lagrange time delay estimation autoregressive model (MLTDEAR). The MLTDEAR technique showed better accuracy to the SNR estimation of a single SEM image, when collated with the AR, first-order interpolation, and nearest neighbourhood models. From the analysed results, MLTDEAR technique has limitations in estimating SNR for image with varying contrast and low magnification ratio.

The shape-preserving cubic Hermite autoregressive moving average (SP2CHARMA) was introduced to estimate the SNR under different noise environments [9].

Later, the adaptive slope nearest neighbourhood (ASNN) model was developed [10]. Slope constants were added into the SNR estimation to improve the accuracy of the result better than using both simple and first-order interpolation.

In 2015, an SNR estimation technique was proposed and named as adaptive tuning piecewise cubic Hermite interpolation (ATPCHIP) [11]. In this ATPCHIP model, a multiplier was implemented to the slope component for adjustment. An improvement to the technique was achieved using the piecewise cubic Hermite interpolation (PCHIP) technique [9].

In 2016, a new technique to SNR was developed called

Manuscript received March 5, 2018; revised June 2018.

K. S. Sim is with the Faculty of Engineering and Technology, Multimedia University, Jalan Ayer Keroh Lama, 75450 Bukit Beruang, Melaka, Malaysia (phone: 606-252-3480; fax: 606-231-6552; e-mail: sksbg2018@gmail.com).

J. W. Leong is with the Faculty of Engineering and Technology, Multimedia University, Jalan Ayer Keroh Lama, 75450 Bukit Beruang, Melaka, Malaysia (e-mail: leongjunwei324@gmail.com).

F. F. Ting is with the Faculty of Engineering and Technology, Multimedia University, Jalan Ayer Keroh Lama, 75450 Bukit Beruang, Melaka, Malaysia (e-mail: sicily.ting@gmail.com).

C. P. Tso is with the Faculty of Engineering and Technology, Multimedia University, Jalan Ayer Keroh Lama, 75450 Bukit Beruang, Melaka, Malaysia (e-mail: cptso@mmu.edu.my).

autocorrelation Levinson–Durbin recursion (ACLDR) model [12]. ACLDR was employed as an estimator to measure and quantify the signal spectrum of corrupted SEM images. Computation of SNR values was performed on both original and quantified images. The ACLDR was compared with three other existing algorithms: namely the nearest neighbourhood, first-order linear interpolation and nearest neighbourhood combined with first-order linear interpolation. The ACLDR model is able to obtain higher accuracy in SNR estimation.

A method named as nonlinear least squares regression (NLLSR) was proposed [13]. Images with various textures properties, contrasts and horizontal field width were applied to test the overall performance of NLLSR method, and it is found to be able to better estimate SNR results up to some extent. This method is still bounded by the properties of the image itself.

A novel technique is now presented to calculate the SNR of SEM images based on cubic spline interpolation combine with linear least square regression (CSILLSR). Through this interpolation, the noiseless zero offset point is found. The SNR of SEM images with various setting such as accelerating voltage, beam diameter, surface tilt and contrasts are measured.

This paper begins with problem formulation, then description on nearest method, linear interpolation method, the combination of these two methods, non-linear least square regression method (NLLSR), autocorrelation Levinson-Durbin recursion (LDR) model, and adaptive slope nearest neighbourhood (ASNN) method. After that, the CSILSRSNR is employed and results compared with these six methods for the SNR estimation. Results are tabulated, discussed, and followed by conclusion.

III. Problem Formulation

Equation (1) is employed to compute SNR value of two images with identical signal pattern uncorrelated with white Gaussian noise [11].

$$A(x,y) = S(x,y) + N(x,y)\,, \tag{1}$$

where A(x,y) is a noisy image signal consisting of actual signal S(x,y) plus the white noise with uniformly distributed power spectral density represented by N(x,y).

The autocorrelation function (ACF) for the two identical images of the identical signal source is shown in Fig. 1, and the SNR is given in (2).

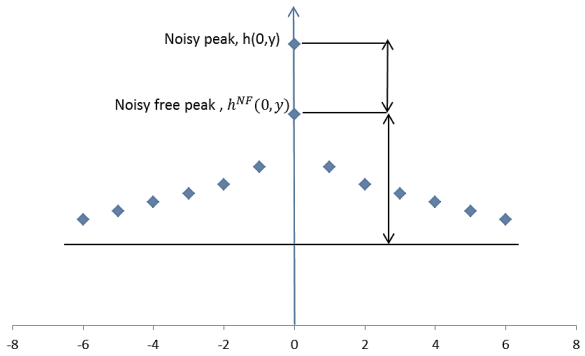

Fig. 1. The ACF of a single image added with white Gaussian noise.

$$SNR = \frac{h^{NF}(0,y)-\mu^2}{h(0,y)-h^{NF}(0,y)}\,, \tag{2}$$

where $h^{NF}(0,y)$ is the noise free peak, $h(0,y)$ is the noisy peak and μ^2 is the mean of the image. Generally, the values of $h(0,y)$ and μ^2 are known, but the value of $h^{NF}(0,y)$ remain unknown. Henceforth, $h^{NF}(0,y)$ is needed to be estimated through a few techniques, which will be discussed next.

IV. Existing Methods

A. Nearest method

This simple method [5] is illustrated in Fig. 2. Two nearest points, h(1,y) and h(-1,y) are located next to the ACF peak. the noise free peak is then given by

$$h^{NN}(0,y) = h(1,y) = h(-1,y)\,. \tag{3}$$

By symmetry, either point is applicable to obtain

$$SNR = \frac{h^{NN}(0,y)-\mu^2}{h(0,y)-h^{NN}(0,y)}\,. \tag{4}$$

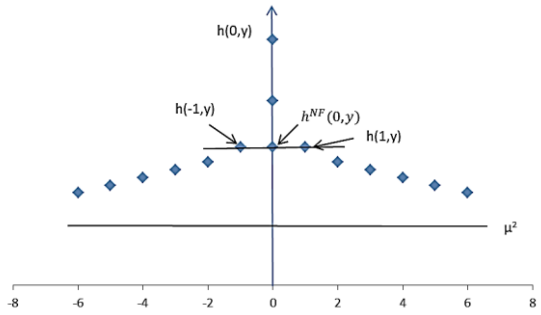

Fig. 2. Nearest method to determine $h^{NF}(0,y)$.

B. Linear interpolation method

In the linear interpolation method [5] illustrated in Fig. 3, two nearest points are taken both before and after the ACF peak. They are *h*(1,y), *h*(2,y), *h*(-1,y), and *h*(-2,y). The interpolate values are

$$h^{int}(0,y) = h(1,y) + [h(1,y) - h(2,y)]$$
$$\text{Or } h^{int}(0,y) = 2[h(1,y)] - h(2,y) \tag{5}$$

$$h^{int}(0,y) = h(-1,y) + [h(-1,y) - h(-2,y)]$$
$$\text{Or } h^{int}(0,y) = 2[h(-1,y)] - h(-2,y) \tag{6}$$

Since these points are similar, either of (5) or (6) can be used for the noise free peak value,

$$SNR = \frac{h^{int}(0,y) - \mu^2}{h(0,y) - h^{int}(0,y)}\,. \tag{7}$$

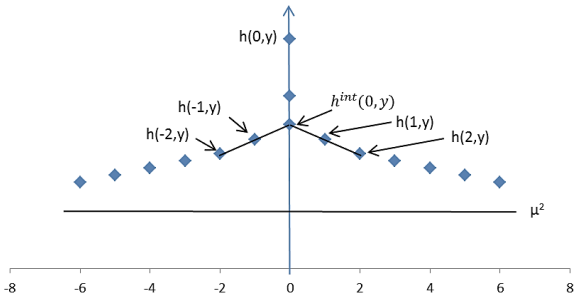

Fig. 3. Linear interpolation method to determine $h^{int}(0,y)$.

C. Combination of linear interpolation and nearest methods (CLIN)

CLIN [13] takes the average result from both linear

interpolation method and nearest method, which is then assigned as the predicted noise free peak $h^{nn+int}(0,y)$. The steps are as below.

$$h^{nn+int}(0,y) = \frac{h^{nn}(0,y)+h^{int}(0,y)}{2} \quad , \tag{8}$$

Equation (9) and (10) are the simplified version of (8).

$$h^{nn+int}(0,y) = \frac{3[h(1,y)]-h(2,y)}{2}, \tag{9}$$

$$h^{nn+int}(0,y) = \frac{3[h(-1,y)]-h(-2,y)}{2} \quad , \tag{10}$$

Either (9) or (10) can be employed into (11) to compute the SNR.

$$SNR = \frac{h^{nn+int}(0,y)-\mu^2}{h(0,y)-h^{nn+int}(0,y)}, \tag{11}$$

D. SNR estimation based on non-linear least square regression

The fourth method is termed non-linear least square regression (NLLSR) [13]. The below (12) shows constant growth or decay where $\bar{h}(0)$is the noise free peak, α is the initial amount, β is the relative growth rate, x is the distance along the x-axis of the ACF curve and the ε is the random white noise.

$$\bar{h}(0) = \hat{y} = (\alpha)\exp(x\beta)\,.\,(e), \tag{12}$$

By taking logarithm, (13) is generated.

$$ln\,(\hat{y}) = \ln(\alpha) + x\beta + \ln\,(e) \tag{13}$$

The first order of NLLSR may be used to estimate the SNR value. Equation (13) can be simplified into (14), where α and β are the constants.

$$\mathrm{h}^{\mathrm{NLLSR}} = \hat{y} = \alpha\,\varepsilon\,(x)^{\beta} \quad , \tag{14}$$

Then, (15) can be utilized to get the SNR value.

$$SNR = \frac{h^{NLLSR}(0,y)-\mu^2}{h(0,y)-h^{NLLSR}(0,y)} = \frac{\alpha\,\varepsilon\,(x)^{\beta}-\mu^2}{h(0,y)-\alpha\,\varepsilon\,(x)^{\beta}}, \tag{15}$$

E. Autocorrelation Levinson-Durbin recursion model

The fifth method to get the SNR is named as autocorrelation Levinson-Durbin recursion (LDR) model [12]. The maximum point is taken as the Levinson order-update coefficient (v_k), and is mapped with the autocorrelation values, a from k = 1 until k = n+1. With the summation of the modelling error, ξ_{n+1}, the value of $\mathrm{h}^{\mathrm{LDR}}(0, y)$ is given by in (16).

$$\mathrm{hLDR}(0,y) = v_1 a_{n+1} + v_2 a_{n+1} + v_3 a_{n+1} + \cdots + v_{n+1} a_{n+1} + \xi_{n+1}\,, \tag{16}$$

$$\mathrm{h}^{\mathrm{LDR}}(0,y) = \sum_{k=1}^{(n+1)} v_k a_{n+1} + \xi_{n+1}\,, \tag{17}$$

With these parameters, the SNR is given by

$$SNR = \frac{h^{LDR}(0,y)-\mu^2}{h(0,y)-h^{LDR}(0,y)}\,. \tag{18}$$

F. Adaptive slope nearest-neighbourhood model

The sixth method is the adaptive slope nearest-neighbourhood (ASNN) model [10], based on observing the relation of the noise free peak and the noisy peak using the nearest-neighbourhood method. The *y*-axis intercept and slope of the linear trend line change according to the noise variance (NV) which varies from 0.001 to 0.01. If the slope of the trend line is *G* the *y*-axis intercept is *C*. The SNR can be obtained from (19).

$$\mathrm{SNR}_{\mathrm{predict}} = (G)*(\mathrm{SNR}_{\mathrm{actual}}) - C \tag{19}$$

The value of $\mathrm{SNR}_{\mathrm{actual}}$ can be determined by using equation (2). Hence, the SNR can be predicted using (19).

V. New Method and Materials

A. Cubic spline interpolation with linear least square regression

Cubic spline interpolation with linear least square regression (CSILLSR) can smoothen the polynomial interpolation and has less error. The method is presented in (20).

$$S_i(x) = a_i + b_i(x-x_i) + c_i(x-x_i)^2 + d_i(x-x_i)^3 \tag{20}$$

Among the data points, each interval would have a discrete cubic function. Thus, the spline S(x) is the function when data points, i=1

$S_1(\mathrm{x}) = a_1 + b_1(x-x_1) + c_1(x-x_1)^2 + d_1(x-x_1)^3$, for $x_1 \le x \le x_2$

Similar, it applies to i=2 and so on.

$S_2(\mathrm{x}) = a_2 + b_2(x-x_2) + c_2(x-x_2)^2 + d_2(x-x_2)^3$, for $x_2 \le x \le x_3$

$S_i(\mathrm{x}) = a_i + b_i(x-x_i) + c_i(x-x_i)^2 + d_i(x-x_i)^3$, for $x_i \le x \le x_{i+1}$

where i = 1, 2, 3, …, a_i is the value of noise free at x_i and $\mathrm{S_i(x)}$ is the cubic function. Equation (20) indicates that 4 coefficients are to be determined. The spline ensures that the exactly data points occur as in (21) and (22).

$$S_i(x_i) = a_i \tag{21}$$

$$S_i(x_{i+1}) = S_{i+1}(x_{i+1}) = a_{i+1} \tag{22}$$

To ensure the S(x) to be smooth, (23) and (24) are required to be.

$$\frac{dS_i}{dx_{i+1}} = \frac{dS_{i+1}}{dx_{i+1}} \tag{23}$$

$$\frac{d^2S_i}{dx_{i+1}^2} = \frac{d^2S_{i+1}}{dx_{i+1}^2} \tag{24}$$

From (24), we have [14]

$$\frac{dS_i}{dx_{i+1}}$$

$=b_i + 2c_i x_{i+1} - 2c_i x_{i+1} x_i + 3d_i x_{i+1}^2 - 6d_i x_{i+1} x_i + 3d_i x_i^2$

$\frac{dS_{i+1}}{dx_{i+1}} = 0$

$\frac{dS_i}{dx_{i+1}} = \frac{dS_{i+1}}{dx_{i+1}}$

And, it yields equation (25),

$$b_i + 2c_i x_{i+1} - 2c_i x_{i+1} x_i + 3d_i x_{i+1}^2 - 6d_i x_{i+1} x_i + 3d_i x_i^2 = 0 \quad (25)$$

From (24), we have [14]

$\frac{d^2 S_i}{dx_{i+1}^2} = 2c_i - 2c_i x_i + 6d_i x_{i+1} - 6d_i x_i$

$\frac{d^2 S_{i+1}}{dx_{i+1}^2} = 0$

$\frac{d^2 S_i}{dx_{i+1}^2} = \frac{d^2 S_{i+1}}{dx_{i+1}^2}$

And, it yields equation (26),

$$2c_i - 2c_i x_i + 6d_i x_{i+1} - 6d_i x_i = 0 \quad (26)$$

To determine the three coefficients (b, c and d), (25), (26) , and (27) are required.

$$S_i(x_{i+1}) = a_i + b_i(x_{i+1} - x_i) + c_i(x_{i+1} - x_i)^2 + d_i(x_{i+1} - x_i)^3 \quad (27)$$

Since the values of x are known and we assume $x_i = x_1$ and $x_{i+1} = x_2$, we can then obtain the value of $S_1(x_1)$ according to (22) which equals to a_1. From (22), the value of $S_1(x_2)$ can be obtained since a_2 is known. According to (27), $S_1(x_2)$ is $a_1 + b_1(x_2 - x_1) + c_1(x_2 - x_1)^2 + d_1(x_2 - x_1)^3$.

Since the values of x_1, x_2, $S_1(x_2)$ and y_1 are known, then by solving (25), (26) and (27) simultaneously, the coefficient b_1, $c_1$and $d_1$can be determined where i = 1 and i+1 = 2.

From (25),we have

$b_1 + 2c_1 x_2 - 2c_1 x_2 x_1 + 3d_1 x_2^2 - 6d_1 x_2 x_1 + 3d_1 x_1^2 = 0$

From (26), we obtain

$2c_1 - 2c_1 x_1 + 6d_1 x_2 - 6d_1 x_1 = 0$

From (27),

$S_1(x_2) = a_1 + b_1(x_2 - x_1) + c_1(x_2 - x_1)^2 + d_1(x_2 - x_1)^3$

For our proposed method, we assume x_1 = M/2 and x_2 = M/2+1 since the size of SEM images are M x M pixels. After determining all the coefficients, we can then estimate $S_1(x)$ value when x = (M+1)/2 by referring to (22). The estimated noise free value which is S_i can be predicted. Equation (28) is employed to estimate the SNR. In this case, the value of $S_i(0, y)$ is the estimated noise free when x = (M+1)/2.

$$SNR = \frac{S_i(0,y) - \mu^2}{h(0,y) - S_i(0,y)}, \quad (28)$$

In (28), $h(0, y)$ indicates the peak of noise, μ^2 indicates the mean. It is followed with linear least square regression as formulated in (24).

$$R_i = \alpha r_i^2 + \beta r_i + \gamma_i + \varepsilon_i \quad , \quad (29)$$

where R_i is the estimated SNR, r_i is the original SNR, α, β and γ are the constant coefficients and ε is the unknown error. Equation (28) and (29) can be combined to generate (30).

$$\frac{S_i(0,y) - \mu^2}{h(0,y) - S_i(0,y)} = \alpha r_i^2 + \beta r_i + \gamma_i + \varepsilon_i \quad , \quad (30)$$

The values of α, β and γ can then be computed using (31).

$$\begin{bmatrix} R1 \\ R2 \\ . \\ . \\ . \\ Rn \end{bmatrix} = \begin{bmatrix} r_1^2 & r_1 & 1 \\ . & . & 1 \\ r_n^2 & r_n & 1 \end{bmatrix} \begin{bmatrix} \alpha \\ \beta \\ \gamma \end{bmatrix} + \begin{bmatrix} \varepsilon 1 \\ \varepsilon 2 \\ . \\ . \\ . \\ \varepsilon n \end{bmatrix} \quad (31)$$

The unknown error (ε) needs to be reduced using in (32).

$$[\min_{\beta} \sum_{k=1}^{N} \varepsilon_k^2 = \min_{\beta} \varepsilon^T \varepsilon] = [\frac{d}{dB} \sum_{k=1}^{N} \varepsilon_k^2 = \frac{d}{dB} \varepsilon^T \varepsilon] = 0, \quad (32)$$

Equation (33) represents equation (29)

$$\boldsymbol{T} = \boldsymbol{XB} + \boldsymbol{\varepsilon} \quad , \quad (33)$$

where

$$\mathbf{X} = \begin{bmatrix} r_1^2 & r_1 & 1 \\ . & . & 1 \\ r_n^2 & r_n & 1 \end{bmatrix}, \quad \boldsymbol{\varepsilon} = \begin{bmatrix} \varepsilon 1 \\ \varepsilon 2 \\ . \\ . \\ . \\ \varepsilon n \end{bmatrix}, \quad \mathbf{T} = \begin{bmatrix} R1 \\ R2 \\ . \\ . \\ . \\ Rn \end{bmatrix}, \quad \boldsymbol{B} = \begin{bmatrix} \alpha \\ \beta \\ \gamma \end{bmatrix}$$

The derivation to minimize the error (ε) is shown in (34) [4].

$let\ \boldsymbol{\varepsilon} = \boldsymbol{T} - \boldsymbol{XB}$

Then

$\varepsilon^T \varepsilon = (T - XB)^T (T - XB)$

$= [T^T T - T^T XB + (XB)^T (XB) - (XB)^T T]$

$= T^T T - T^T XB + B^T X^T XB - B^T X^T T$

Therefore

$\frac{d}{d\boldsymbol{B}} (\boldsymbol{\varepsilon^T \varepsilon}) = 0$

$-\boldsymbol{T^T X} + 2\boldsymbol{B^T X^T X} - \boldsymbol{X T^T} = 0$

Solving for B gives

$$\boldsymbol{B} = (\boldsymbol{X^T X})^{-1} \boldsymbol{X^T T} \quad (34)$$

Then, (35) is then used to predict the SNR.

$$R_i = \alpha r_i^2 + \beta r_i + \gamma_i \quad (35)$$

where R_i is the predicted SNR and r_i is the original SNR.

The algorithm of the proposed method is shown as Algorithm 1.

Algorithm 1 Cubic spline interpolation with linear least square regression (CSILLSR)

1: ASET [y,x] to obtain the size of the input image.
2: Display the input image.
3: SET fn_d1 with imnoise function to corrupt the input image with noise.
4: Display the corrupted image.
5: SET j6 to obtain the input image after fast Fourier transform.
6: SET j8 to obtain the corrupted image after fast Fourier transform.
7: Plot the ACF curve of j6.
8: Plot the ACF curve of j8.
9: SET actual_SNR_dB to calculate the actual SNR value.
10: SET INT_SNR_dB to calculate the SNR value using first order interpolation method.
11: SET NBH_SNR_dB to calculate the SNR value using nearest neighbourhood method.
12: SET INTNN_SNR_dB to calculate the SNR value using the combination of first order interpolation and nearest neighbourhood method.

13: SET CSISGWLSE_SNR_dB to calculate the SNR value using cubic method.
14: SET CSILSRSNR_dB to calculate the SNR value using CSILSRSNR method.
15: SET noisefree_peak as the noise free peak value.
16: END

VI. Results and Discussion

A. *Performance of CSILLSR method versus other existing methods*

Six types of noiseless SEM images of size 256 x 256 pixels resolution are used, as shown in Fig. (4). The six existing methods are nearest, linear interpolation, the combination of linear interpolation and nearest method, NLLSR, autocorrelation LDR, and ASNN. They are compared with the *CSILLSR*.

First, the original SEM image (without noise) is degraded or corrupted with additional white noise. The noise variance was varied from the ranges of 0.001 to 0.010. The comparison between the original and the estimated SNR values over this noise variance range is shown in Tables 1 to 6. The first column in the tables was represented by the value of the noise variance and the second column refers to the SNR value. The rest of the columns clearly indicate the SNR values using the other methods.

In order to validate the performance of presented technique, 250 noise free images are employed for the SNR estimation. Henceforth, only 6 samples out of 250 SEM images are presented in this paper as shown in Fig. 4. The experimental results are tabulated and plotted in graph. The performance of the SNR estimation is measured by the application of absolute error.

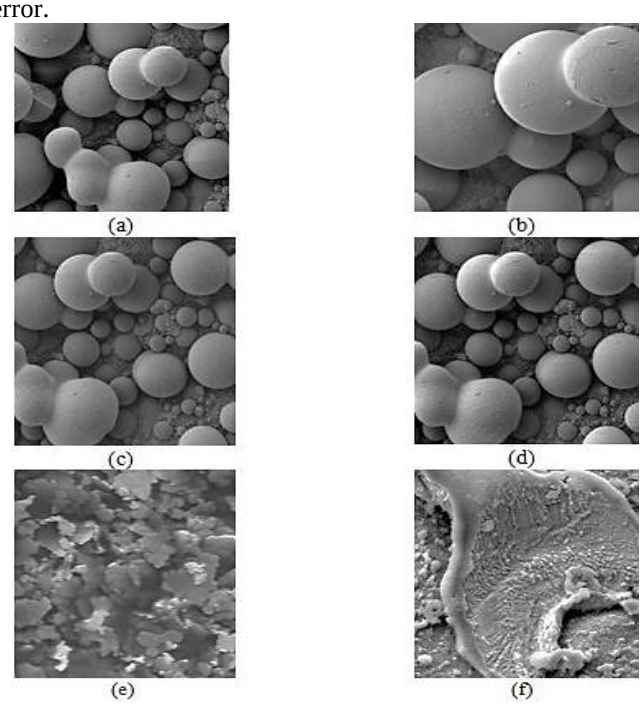

Fig. 4. (a) IC compound at horizontal field-width = 50μm, (b) IC compound at horizontal field-width = 25μm, (c)222nm aperture size IC compound image, (d) 89nm aperture size IC compound image, (e) The material image A and (f) The material image B.

Referring to the results obtained from six figures, when the noise variance is 0.001, most methods are more liable to overestimate or underestimate the SNR. The characteristics of the image may lead to the overestimation or underestimation issues. The characteristic of image includes aperture size, magnification ratio and so on. The results for 6 figures are tabulated in Tables I to VI.

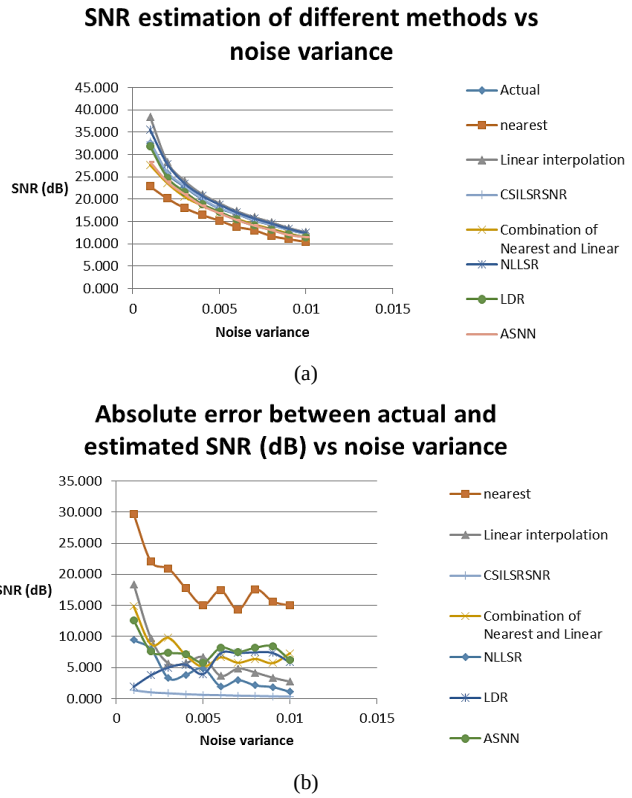

Fig. 5. IC compound at horizontal field-width= 50μm in Fig. 4(a). (a) SNR versus noise variance. (b) Absolute error versus noise variance.

From the tables, nearest method appears to underestimate the SNR value, because the method takes the nearest point from the ACF peak as the noiseless peak. Fig. 5(b) to Fig. 10(b) show that this method gives the greatest relative error compared to others. The stability and accuracy are poor, and it is highly dependent on image properties.

For the linear interpolation method, according to Tables 1 to 6, it tends to overestimate the SNR value. As shown in (b) of Fig. 5 to Fig. 10 at the noise variance of 0.001. The accuracy of linear interpolation method is low when the noise variance is lesser than 0.002 and it might upwardly concave to indicate overestimation. This problem arises because of the properties of the images and the values of the unpredicted errors which refer to the existence of the white Gaussian noise. However, the linear interpolation method is more accurate than the nearest method. The SEM image textures, contrasts, magnification ratio, and aperture size are referred to as the nature or the properties of the image in this context.

The combination of these two methods by taking the average of both techniques is shown in (b) of Fig. 5 to Fig. 10. But this method also shows poor accuracy compared to linear interpolation, as seen in Tables I to VI.

The NLLSR method shows poor estimation of the SNR results in Tables III to VI, which might be due to the relative growth or decay of the ACF pattern. In (b) of Fig. 7 to Fig. 10, it has slightly higher difference in error as compared to the other methods.

Although the LDR has better SNR estimation than nearest method, linear interpolation, the combination of nearest method and linear interpolation as well as the NLLSR, it still carries certain absolute error varying from 1dB to 1.14dB.

For ASNN, it shows poor estimation of the SNR results in Tables I-VI. It may due to the relative growth or decay of the

ACF pattern that cater around the noiseless peak. In (b) of Fig. 5 to Fig. 10, it has slightly high error difference which varies from 1 to 11.5 dB.

The absolute error in there is obtained from Tables I to VI. From Fig. 5(b) and Fig. 6(b) of IC compound at horizontal field-width = 50μm and IC compound at horizontal field-width = 25μm images, it can be seen that with the noise variance range, the error difference of CSILLSR varies from 0.04 to 0.4 dB for IC compound A image and 0.05 to 0.5 dB for the IC compound B image.

In Fig. 7(b) and Fig. 8(b) of the IC compound image captured by 222 nm of aperture size and the IC compound image with 89 nm of aperture size, as the noise variance was being altered from 0.001 to 0.010. The error difference of CSILLSR method varies from 0.013 to 0.33 dB for the IC compound image captured by 222 nm of aperture size and 0.06 to 0.48 dB for the IC compound image captured by 89 nm of aperture size.

Furthermore, in Fig. 9(b) and Fig. 10(b), at the same noise variance range, the error difference of CSILLSR varies from 0.07dB to 0.3 dB for material image A and 0.05 dB to 0.52 dB for material image B.

From the results of the absolute error from (b) of Fig. 5 to Fig. 10 of CSILLSR, clearly the absolute error is less than 1 dB, implying better stability and compared to the other six methods.

The accuracy of CSILLSR relies on the N points selections. In addition, the second order method needs calculations of optimal α, β, and γ coefficients. (See equation (38)). These coefficients are able to provide better fitting to estimate the SNR values.

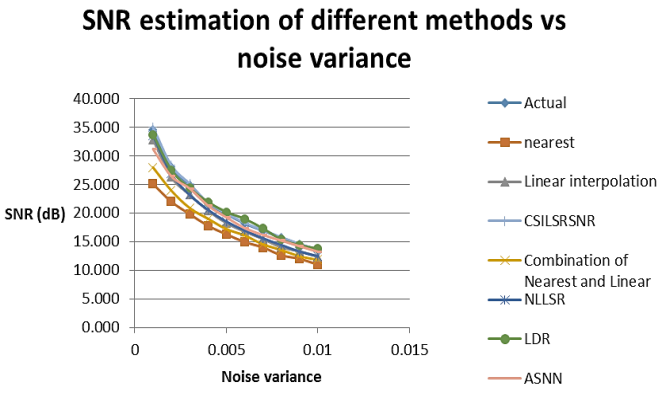

(a)

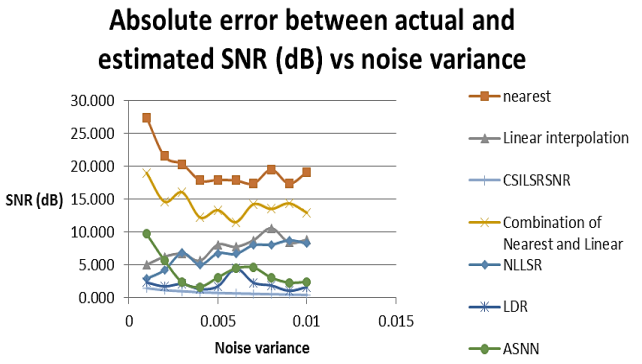

(b)

Fig. 6. Graphs for IC compound at horizontal field-width = 25μm mages in Fig. 4.(b) (a) SNR estimation against noise variance, and (b) Absolute error against noise variance.

The performance of presented work, CSILLSR is bench marked with state-of the art methods. Estimation error measurement metric is applied. Tabulated results show that CSILLSR outperformed other state of the art methods by having nearest SNR estimation to the actual SNR of the SEM images.

The estimation ratio is suggested by researcher to determine the performance of the image noise estimation techniques [16], as shown in (36).

$$estimation\ ratio = \frac{\sigma_{estimated}}{\sigma_{Actual\ SNR}}, \tag{36}$$

Where $\sigma_{estimated}$ defines estimated SNR and $\sigma_{Actual\ SNR}$ is the actual SNR of the SEM images.

If estimation ratio is equal to 1, it indicates the estimated noise variance, $\sigma_{estimated}$ is the identical to actual SNR of the image. The closer the estimation ratio equal to 1, the higher the accuracy of the SNR estimation method.

For the results in Fig. 5 to 10, the nearest method seems to give the most absolute error. The linear interpolation has less accuracy, although it has better results than the nearest method. However, the combination of linear interpolation and nearest method produces lesser SNR accuracy, which may be due to the reliance on the properties and the nature of image. For better accuracy, the cubic spline interpolation cascaded with the linear least square regression is best. Overall, CSILLSR method provides better accuracy and stability. Fig. 11 shows the designed application based on presented CSILLSR.

B. Accelerating voltage

Fig. 12 shows 3 material SEM images captured from 10 – 30 keV. By increasing the voltage, the image contrast increases too. When the accelerating voltage is reduced, the image contrast is also reduced. The ACF curve is shown in Figure 13. The results obtained from various accelerating voltages are also tabulated in Table VII.

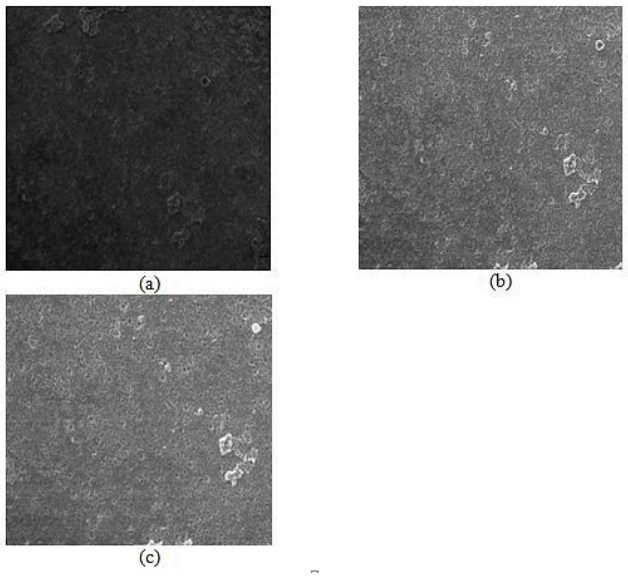

Fig. 12. Material image at (a) 10keV, (b) 20keV and (c) 30keV

TABLE I
SNR ESTIMATION COMPARISON OF IC COMPOUND IMAGE AT HORIZONTAL FIELD-WIDTH = 50μm IN DECIBEL (DB)

Noise Variance	Actual SNR	Nearest	Linear Interpolation	CLIN	NLLSR	LDR	ASNN	CSILLSR	Estimation Error
0.001	**32.477**	22.837	38.445	27.656	35.534	31.851	28.380	**32.917**	**1.0135**
0.002	**25.825**	20.139	28.321	23.573	27.875	24.851	23.869	**26.088**	**1.0102**
0.003	**22.758**	17.998	24.049	20.529	23.506	21.616	21.083	**22.956**	**1.0087**
0.004	**19.992**	16.445	21.139	18.596	20.760	18.902	18.567	**20.138**	**1.0073**
0.005	**17.898**	15.205	19.097	16.983	18.773	17.189	16.857	**18.010**	**1.0063**
0.006	**16.691**	13.788	17.305	15.581	17.026	15.469	15.326	**16.786**	**1.0057**
0.007	**15.236**	13.056	15.973	14.354	15.690	14.119	14.090	**15.311**	**1.0049**
0.008	**14.241**	11.742	14.840	13.331	14.545	13.179	13.073	**14.304**	**1.0044**
0.009	**13.090**	11.045	13.532	12.341	13.334	12.128	11.989	**13.141**	**1.0039**
0.01	**12.255**	10.421	12.591	11.358	12.389	11.540	11.497	**12.297**	**1.0034**

TABLE II
SNR estimation comparison of IC compound image at horizontal field-width = 25μm in decibel (dB)

Noise Variance	Actual SNR	Nearest	Linear Interpolation	CLIN	NLLSR	LDR	ASNN	CSILSR	Estimation Error
0.001	**34.518**	25.068	32.789	27.967	33.525	33.721	31.179	**35.021**	**1.0146**
0.002	**28.010**	21.984	26.269	23.919	26.835	27.531	26.422	**28.327**	**1.0113**
0.003	**24.860**	19.808	23.202	20.877	23.173	24.343	24.282	**25.102**	**1.0097**
0.004	**21.642**	17.780	20.425	19.004	20.557	21.921	21.291	**21.818**	**1.0081**
0.005	**19.847**	16.292	18.248	17.204	18.507	20.190	19.239	**19.990**	**1.0072**
0.006	**18.176**	14.935	16.771	16.090	16.969	18.981	17.369	**18.292**	**1.0064**
0.007	**16.936**	13.996	15.457	14.528	15.583	17.322	16.162	**17.034**	**1.0058**
0.008	**15.672**	12.620	14.016	13.557	14.411	15.383	15.195	**15.753**	**1.0052**
0.009	**14.530**	12.009	13.312	12.446	13.264	14.379	14.197	**14.596**	**1.0045**
0.01	**13.567**	10.978	12.373	11.814	12.446	13.785	13.241	**13.622**	**1.0041**

TABLE III
SNR ESTIMATION COMPARISON OF IC COMPOUND IMAGE WITH 222NM OF APERTURE SIZE

Noise Variance	Actual SNR	Nearest	Linear Interpolation	CLIN	NLLSR	LDR	ASNN	CSILSR	Estimation Error
0.001	**28.624**	19.024	22.206	20.500	21.648	28.212	21.909	**28.956**	**1.0116**
0.002	**22.461**	16.379	18.626	17.499	18.261	22.145	16.396	**22.653**	**1.0085**
0.003	**19.068**	14.303	16.113	15.273	15.941	18.855	14.048	**19.198**	**1.0068**
0.004	**16.581**	12.793	14.364	13.435	14.006	16.318	12.742	**16.673**	**1.0055**
0.005	**14.503**	11.426	12.656	11.988	12.463	14.832	11.449	**14.569**	**1.0046**
0.006	**12.955**	10.147	11.311	10.757	11.248	12.626	9.989	**13.003**	**1.0037**
0.007	**11.711**	9.197	10.149	9.643	10.092	11.477	8.984	**11.748**	**1.0032**
0.008	**10.523**	8.166	9.202	8.734	9.053	10.369	8.027	**10.550**	**1.0026**
0.009	**9.544**	7.358	8.179	7.878	8.175	9.319	6.914	**9.563**	**1.0020**
0.01	**8.620**	6.662	7.453	7.053	7.374	8.483	6.524	**8.633**	**1.0015**

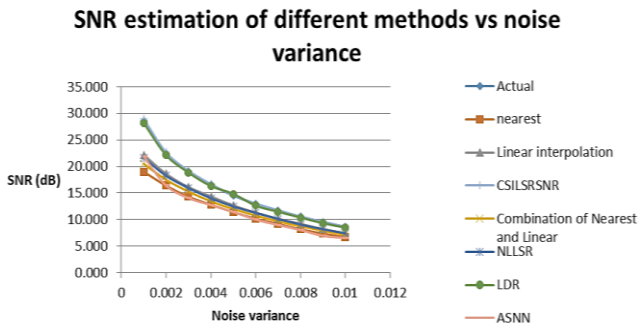

(a)

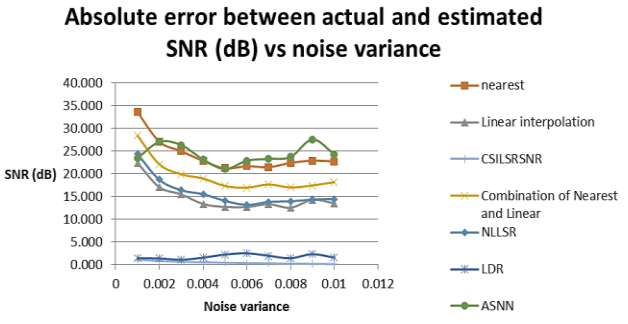

(b)

Fig. 7. Graphs for 222nm aperture size IC compound image in Fig. 4 (c). (a) SNR estimation versus noise variance, and (b) The absolute error versus noise variance.

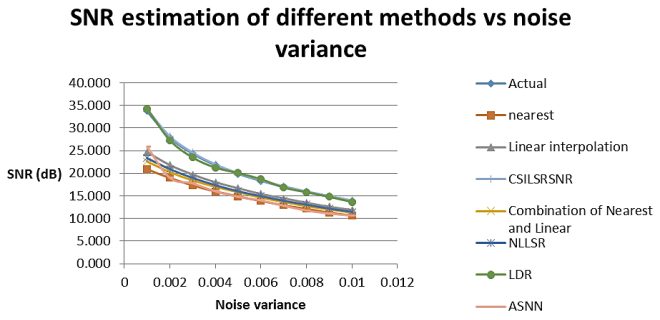

(a)

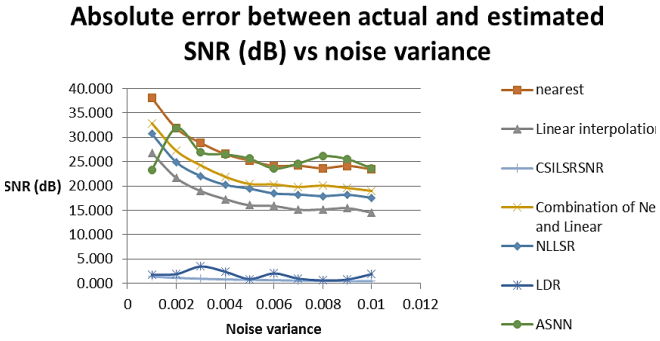

(b)

Fig. 8. Graphs for 89nm aperture size IC compound image in Fig. 4 (d). (a) The SNR estimation versus noise variance, and (b) The absolute error versus noise variance.

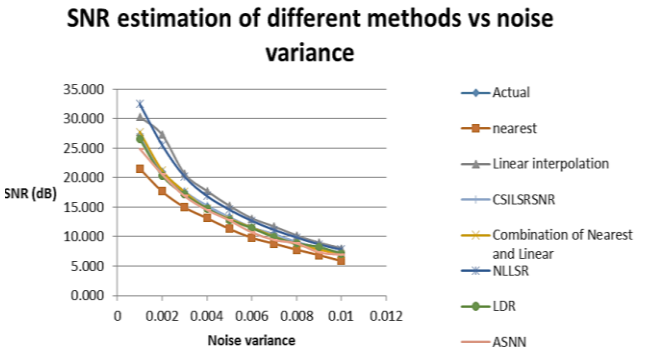

(a)

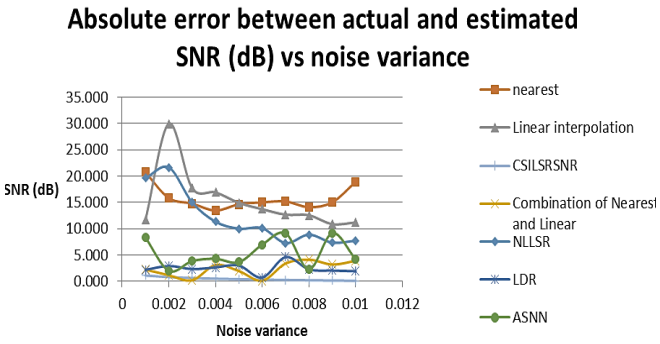

(b)

Fig. 9. Graphs for material image A in Fig. 4 (e). (a)The SNR estimation versus noise variance, and (b)The absolute error versus noise variance.

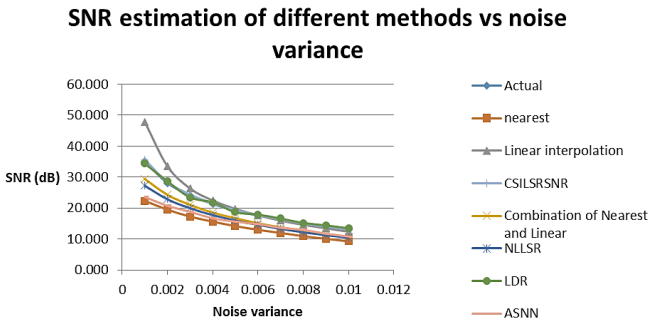

(a)

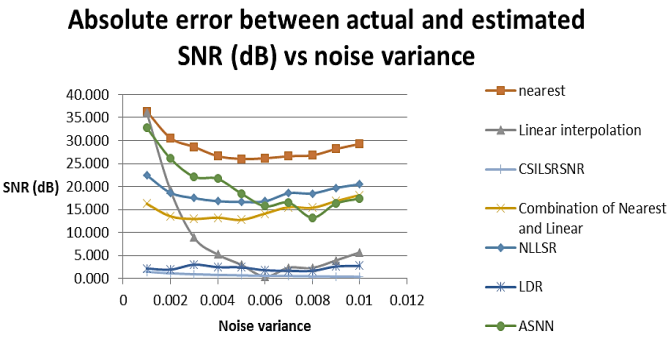

(b)

Fig. 10. Graphs for material image B in Fig. 4 (f). (a) The SNR estimation using various methods versus noise variance, and (b) The absolute error versus noise variance.

TABLE VII
RESULTS FOR MATERIAL IMAGE CAPTURED AT THREE ACCELERATING VOLTAGES

Voltage (keV)	Noise ACF at zero offset point	**CSILLSR noise-free ACF at zero offset point**	Mean	Signal	Signal (dB)
10	4442.797	**4436.443**	3850.460	585.983	39.297
20	18150.156	**18124.201**	15160.070	2964.131	41.154
30	23206.060	**23172.875**	19148.496	4024.379	41.675

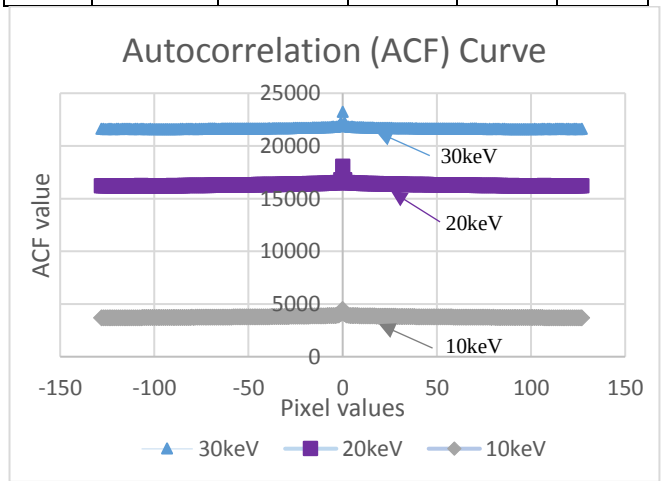

Fig. 13. The ACF curve of sample images captured at three accelerating voltages from 10 keV to 30 keV

TABLE IV
SNR ESTIMATION COMPARISON OF IC COMPOUND IMAGE WITH 89NM OF APERTURE SIZE

Noise Variance	Actual SNR	Nearest	Linear Interpolation	CLIN	NLLSR	LDR	ASNN	CSILSR	Estimation Error
0.001	**33.705**	20.871	24.674	22.618	23.350	34.303	25.858	**34.182**	**1.0142**
0.002	**27.848**	18.977	21.820	20.263	20.912	27.318	18.977	**28.161**	**1.0112**
0.003	**24.339**	17.320	19.722	18.439	18.977	23.497	17.767	**24.569**	**1.0094**
0.004	**21.784**	15.999	18.016	17.011	17.374	21.262	16.012	**21.963**	**1.0082**
0.005	**19.880**	14.870	16.692	15.821	16.012	20.058	14.791	**20.024**	**1.0072**
0.006	**18.329**	13.906	15.419	14.605	14.944	18.703	14.004	**18.448**	**1.0065**
0.007	**17.029**	12.915	14.455	13.655	13.921	16.864	12.836	**17.128**	**1.0058**
0.008	**15.914**	12.152	13.499	12.719	13.060	15.818	11.762	**15.998**	**1.0053**
0.009	**14.907**	11.311	12.606	11.985	12.196	14.789	11.103	**14.978**	**1.0048**
0.01	**13.940**	10.676	11.912	11.293	11.490	13.674	10.650	**13.999**	**1.0042**

TABLE V
SNR ESTIMATION COMPARISON OF MATERIAL IMAGE A

Noise Variance	Actual SNR	Nearest	Linear Interpolation	CLIN	NLLSR	LDR	ASNN	CSILSR	Estimation Error
0.001	**27.168**	21.542	30.336	27.771	32.494	26.579	24.912	**27.464**	**1.0109**
0.002	**20.987**	17.666	27.272	21.226	25.530	20.378	20.571	**21.151**	**1.0078**
0.003	**17.556**	14.964	20.662	17.589	20.189	17.149	16.883	**17.662**	**1.0060**
0.004	**15.172**	13.133	17.736	14.703	16.889	14.771	14.525	**15.246**	**1.0049**
0.005	**13.248**	11.309	15.224	12.990	14.572	12.852	12.768	**13.300**	**1.0039**
0.006	**11.528**	9.799	13.108	11.541	12.691	11.448	10.726	**11.563**	**1.0030**
0.007	**10.384**	8.809	11.699	10.034	11.139	9.908	9.440	**10.410**	**1.0025**
0.008	**9.059**	7.783	10.195	8.687	9.862	8.853	8.855	**9.075**	**1.0018**
0.009	**8.085**	6.871	8.963	7.828	8.678	8.249	7.346	**8.096**	**1.0014**
0.01	**7.240**	5.872	8.050	6.959	7.799	7.103	6.937	**7.247**	**1.0010**

TABLE VI
SNR COMPARISON OF MATERIAL IMAGE B

Noise Variance	Actual SNR	Nearest	Linear Interpolation	CLIN	NLLSR	LDR	ASNN	CSILSR	Estimation Error
0.001	**35.152**	22.359	47.860	29.435	27.246	34.383	23.620	**35.674**	**1.0148**
0.002	**28.118**	19.516	33.530	24.311	22.871	28.664	20.774	**28.438**	**1.0114**
0.003	**24.209**	17.278	26.367	21.073	19.978	23.478	18.848	**24.437**	**1.0094**
0.004	**21.361**	15.671	22.478	18.532	17.767	21.890	16.728	**21.532**	**1.0080**
0.005	**19.197**	14.204	19.770	16.746	16.001	18.731	15.650	**19.329**	**1.0069**
0.006	**17.610**	13.005	17.682	15.122	14.653	17.927	14.841	**17.718**	**1.0061**
0.007	**16.362**	12.008	15.976	13.822	13.328	16.638	13.661	**16.452**	**1.0055**
0.008	**14.964**	10.955	14.619	12.663	12.194	15.215	12.983	**15.035**	**1.0047**
0.009	**14.056**	10.095	13.499	11.689	11.285	14.425	11.762	**14.117**	**1.0043**
0.01	**13.152**	9.302	12.406	10.765	10.458	13.515	10.863	**13.203**	**1.0039**

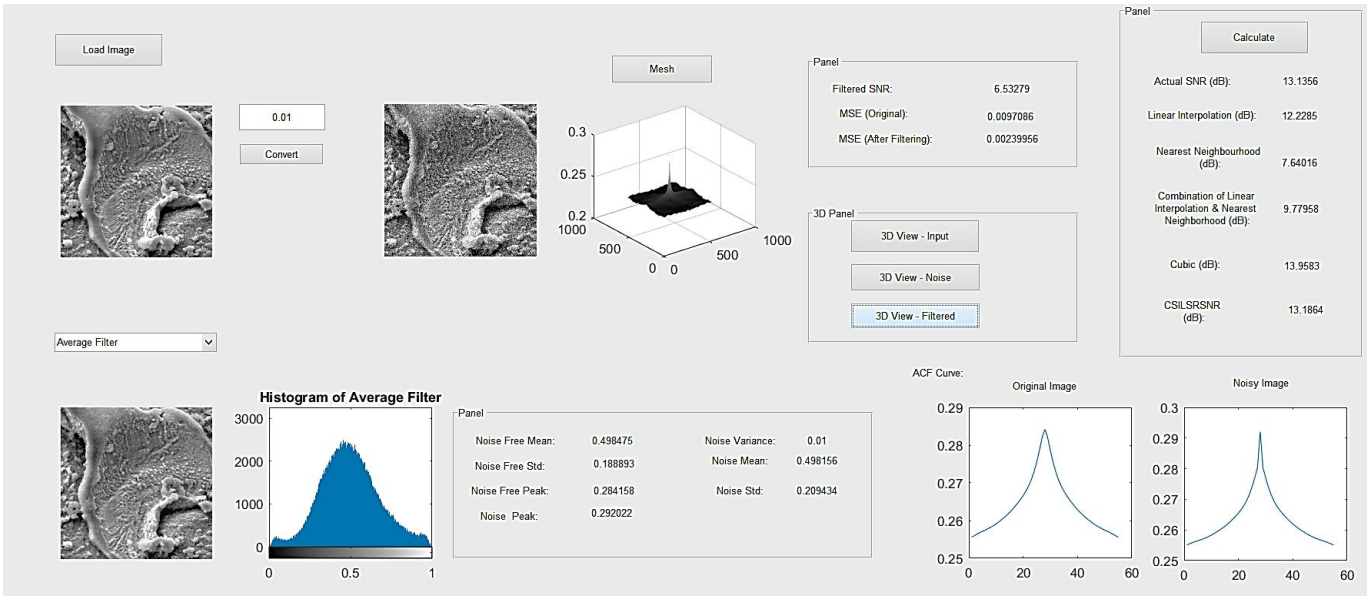

Fig. 11. The designed application for CSILLSR.

C. Beam diameter

The beam diameter is also a key factor in affecting the shape ACF curve. The spatial resolution of the image increases when the probe size decreases. Four samples of IC compound images are captured with 60 nm to 18 nm beam diameter and shown in Fig. 14. The results in Table VIII shows that as the beam diameter increases, the better is the contrast of image. Thus, SEM images with finer beam diameter would contain more noise signal, which results in worse contrast. The ACF curve is shown in Fig. 15.

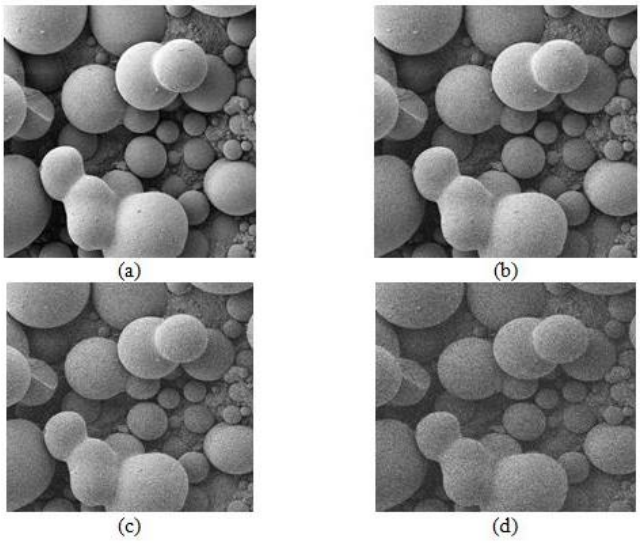

Fig. 14. IC compound image with various beam diameter (a) 60nm, (b)38nm, (c) 25nm and (d) 18nm

TABLE VIII
RESULTS FOR IC COMPOUND IMAGE CAPTURED AT VARIOUS BEAM DIAMETERS

Beam Diameter (nm)	Noisy ACF	Noise Free	Mean	Signal	Signal (dB)	Noise	SNR
60	16247.854	16224.620	13046.962	3177.657	42.720	23.234	136.765
38	15029.429	15007.937	12569.624	2438.313	41.096	21.492	113.452
25	14815.807	14794.620	12719.551	2075.069	39.819	21.187	97.943
18	11842.271	11825.336	10373.616	1451.720	38.662	16.934	85.726

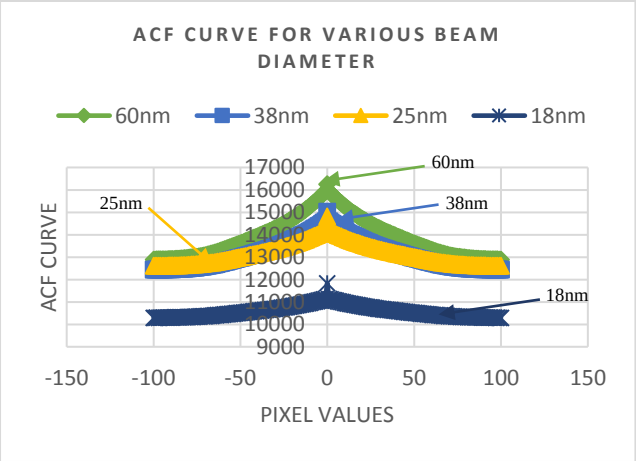

Fig. 15. The ACF curve of IC compound images captured at four beam diameters from 60nm to 18nm.

D. Surface tilt

The Fig. 16 is taken when the surface of the SEM images are tilted at 0°, 10° and 20°. The images in Fig. 15, show that greater tilt angle, will result in higher ACF value. Thus, the ACF value is at the highest for the image with tilt angle of 20°. The ACF curve is illustrated in Fig. 17 and the results are tabulated in Table IX.

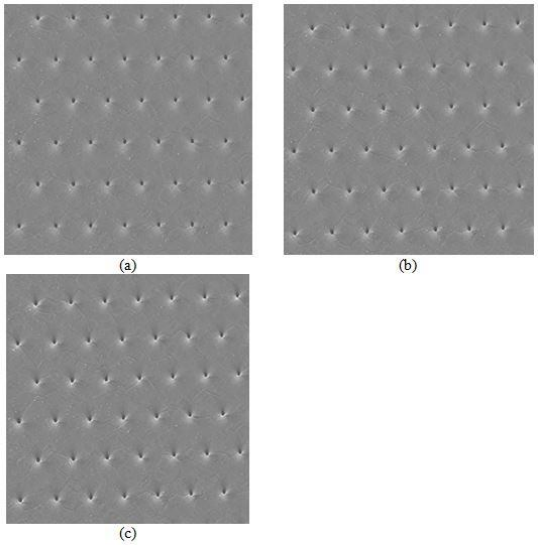

Fig. 16. Power IC package cell image with (a) tilt angle of 0°, (b) tilt angle of 10° and (c) tilt angle of 20°.

TABLE IX
RESULTS FOR POWER IC PACKAGE IMAGES CAPTURED AT VARIOUS TILT ANGLES

Tilt Angle (°)	Noisy ACF	Noise Free	Mean	Signal	Signal (dB)	Noise	SNR
0	18487.543	18461.106	18367.324	93.782	10.998	26.437	3.547
10	18531.158	18504.658	18404.092	100.566	11.584	26.500	3.795
20	18603.169	18576.567	18451.581	124.986	13.439	26.603	4.698

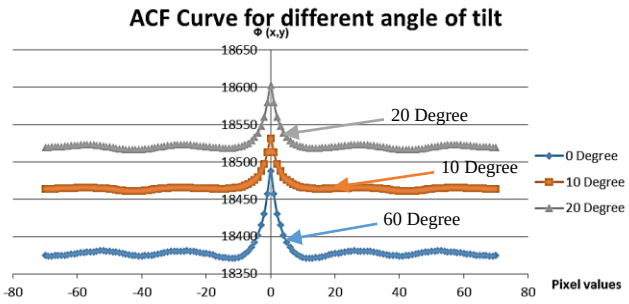

Fig. 17. The ACF curve of cell of power IC package images captured at three tilt angles.

E. Contrast in SEM images

The image contrast can be adjusted by modifying the value of the accelerating voltages. Referring to Table X, three samples of images from mould compound of power IC package are taken at three different contrasts and are shown in Fig. 18. From the results, the ACF value is the highest for high contrast image, then followed by middle contrast and low contrast. Fig.19 shows the corresponding ACF curve.

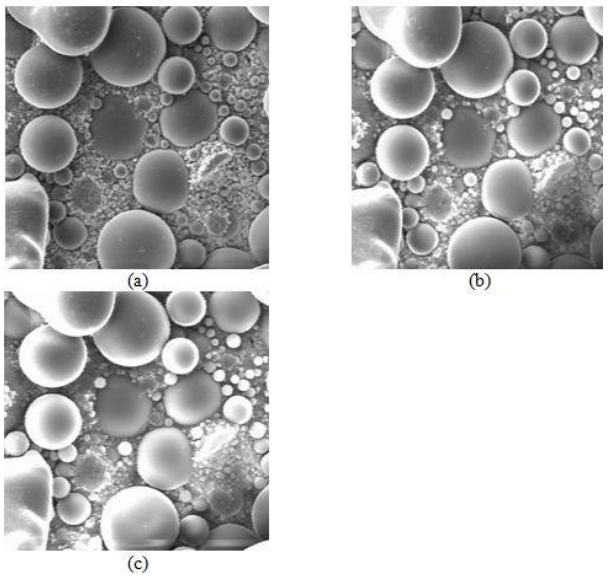

Fig. 18. Power IC package mould compound image with (a) low contrast, (b) middle contrast and (c) high contrast.

TABLE X
RESULTS FOR POWER IC PACKAGE IMAGES CAPTURED AT VARIOUS CONTRASTS

Contrast	Noisy ACF	Noise Free	Mean	Signal	Signal (dB)	Noise	SNR
Low	24520.048	24484.984	19843.827	4641.158	42.435	35.064	132.364
Middle	30625.369	30581.575	23703.966	6877.609	43.920	43.794	157.044
High	33491.077	33443.185	25117.771	8325.414	44.803	47.892	173.836

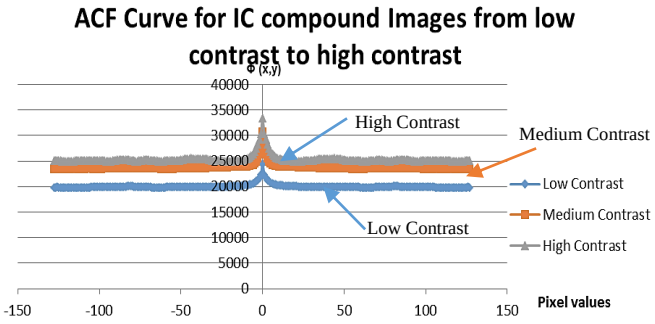

Fig. 19. The ACF curve of power IC package mould compound images captured at three contrast values.

VII. PERFORMANCE OF CSILLSR METHOD VERSUS CRAMER – RAO LOWER BOUND

In this section, we apply the Cramer-Rao Lower Bound to test the performance of CSILLSR with other techniques for the six images. The CRLB is an approach to acquire the lower bound of the mean squared error (MSE). If the estimator performance is equivalent or slightly greater than the CRLB, the estimator can be concluded as a good estimator [7] [15].

Figs. 20-25 show that the CSILLSR is well performed for IC compound at horizontal field-width = 50 μm, IC compound at horizontal field-width = 25μm, 222 nm aperture size IC compound image, 89 nm aperture size IC compound image, The material image A and The material image B are better than those from the other methods. The error variances of CSILLSR are less than 0.1% different from the CRLB.

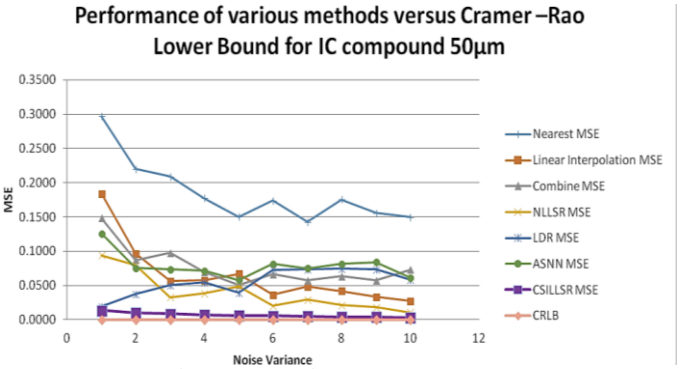

Fig. 20. Graph of MSE values of various methods against Cramer-Rao lower bound for IC compound at 50 μm.

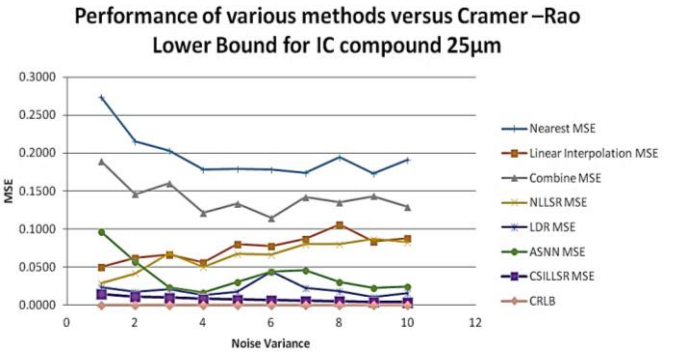

Fig. 21. Graph of MSE values of various methods against Cramer-Rao lower bound for IC compound at 25 μm.

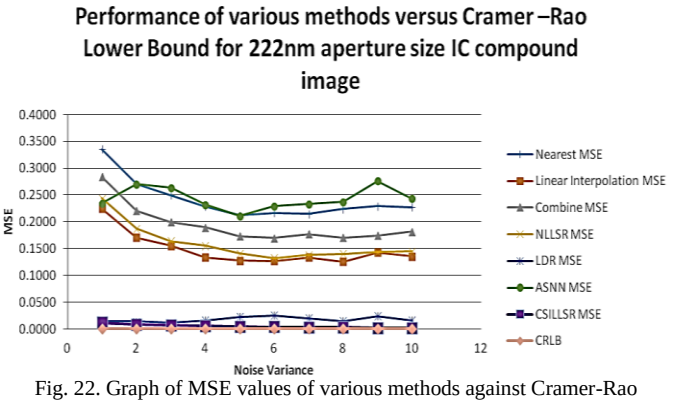

Fig. 22. Graph of MSE values of various methods against Cramer-Rao lower bound for 222nm aperture size IC compound image.

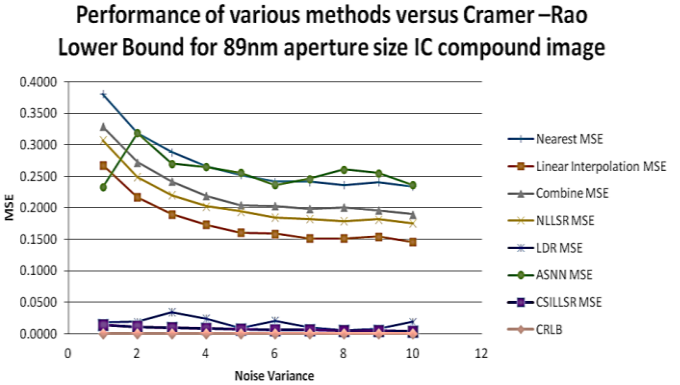

Fig. 23. Graph of MSE values of various methods against Cramer-Rao lower bound for 89nm aperture size IC compound image.

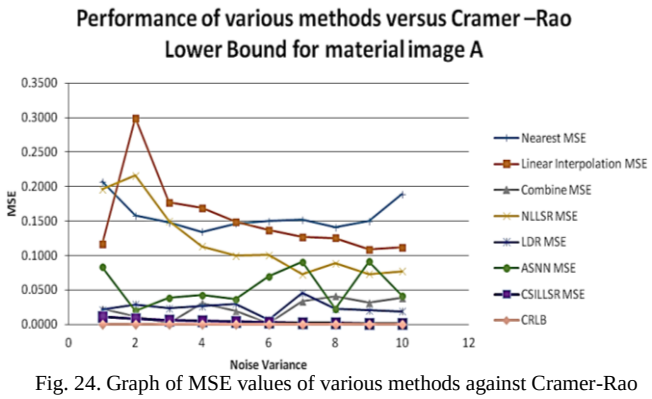

Fig. 24. Graph of MSE values of various methods against Cramer-Rao lower bound for material image A.

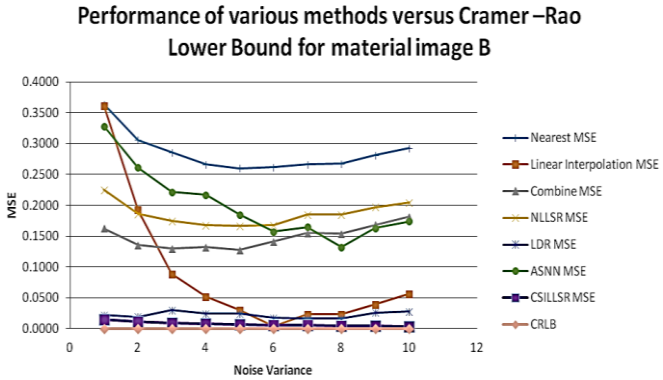

Fig. 25. Graph of MSE values of various methods against Cramer-Rao lower bound for material image B.

VIII. Cubic Spline Interpolation with Linear Least Square Regression Wiener filter

In this section, for the purpose of applications, three filters namely Cubic Spline Interpolation with Linear Least Square Regression Wiener filter, Average filter and Median filter are introduced. Mean Square Error (MSE) is then measured for three filters to compare its performances. Four SEM images with the size of 256 x 256 pixels are applied. The noise variances are implemented from the range of 0.001 to 0.003.

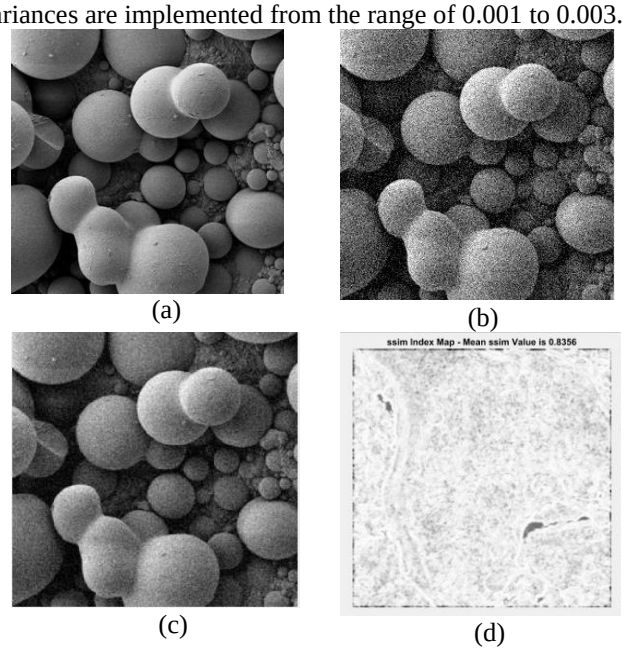

(a) (b) (c) (d)

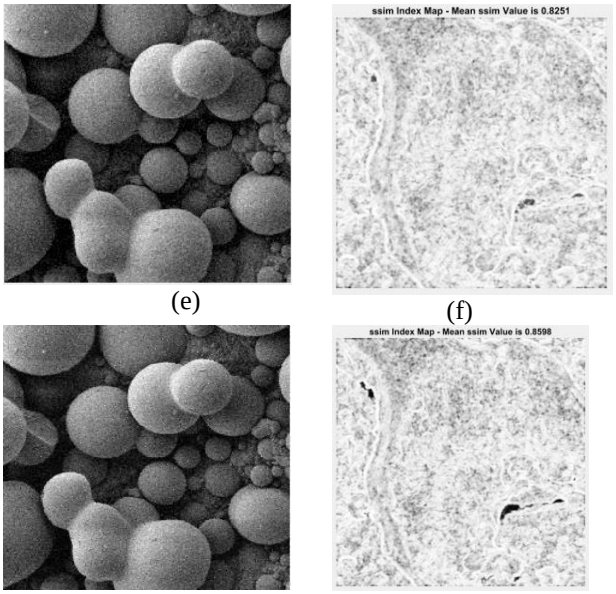

(e) (f) (g) (h)

Fig. 26. (a) Original IC compound A, (b) Corrupted IC compound A with noise, (c) Average filtered image, (d) The SSIM index map of (c), (e) Median filtered image, (f) The SSIM index map of (e), and (g) Wiener (CSILLSR) filtered image and (h) The SSIM index map of (g).

TABLE XI
MSE OF IC COMPOUND A IMAGE

Noise Variance	Average filter (MSE)	Median filter (MSE)	**Wiener filter (MSE)**
0.001	0.000402	0.000290	**0.000229**
0.002	0.000515	0.000470	**0.000393**
0.003	0.000625	0.000639	**0.000566**

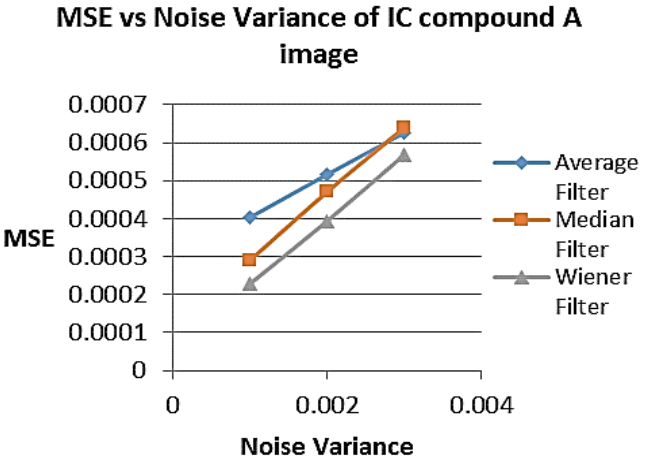

Fig. 27. Graph of MSE for three types of filters vs Noise Variance for IC compound A in Fig. 26

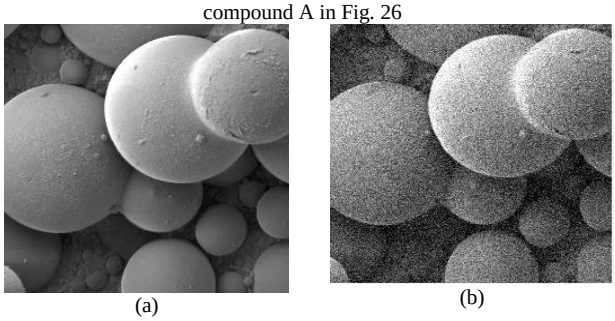

(a) (b)

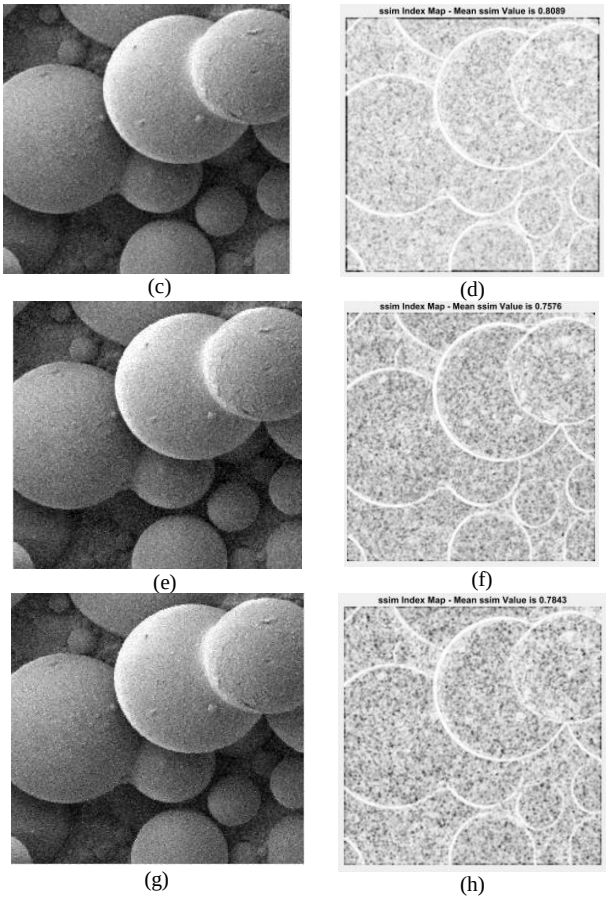

Fig. 28. (a) Original IC compound B, (b) Corrupted IC compound B with noise, (c) Average filtered image, (d) The SSIM index map of (c), (e) Median filtered image, (f) The SSIM index map of (e), and (g) Wiener (CSILLSR) filtered image and (h) The SSIM index map of (g).

TABLE XII
MSE OF IC COMPOUND B IMAGE

Noise Variance	Average filter (MSE)	Median filter (MSE)	**Wiener filter (MSE)**
0.001	0.000341	0.000258	**0.000197**
0.002	0.000454	0.000442	**0.000366**
0.003	0.000567	0.000619	**0.000548**

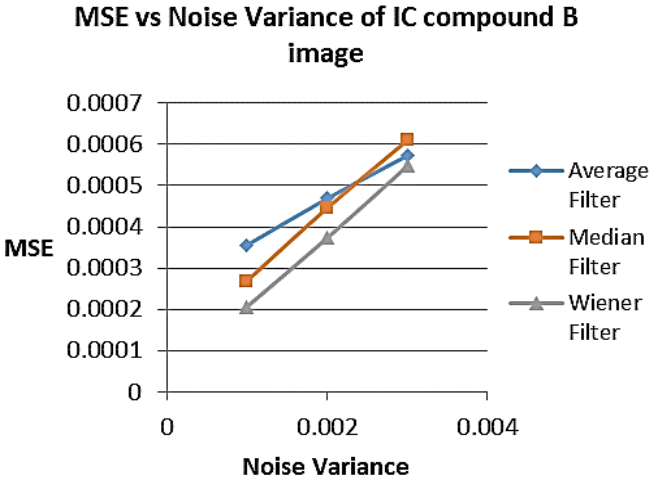

Fig. 29. Graph of MSE for three types of filters vs Noise Variance for IC compound B in Fig. 28

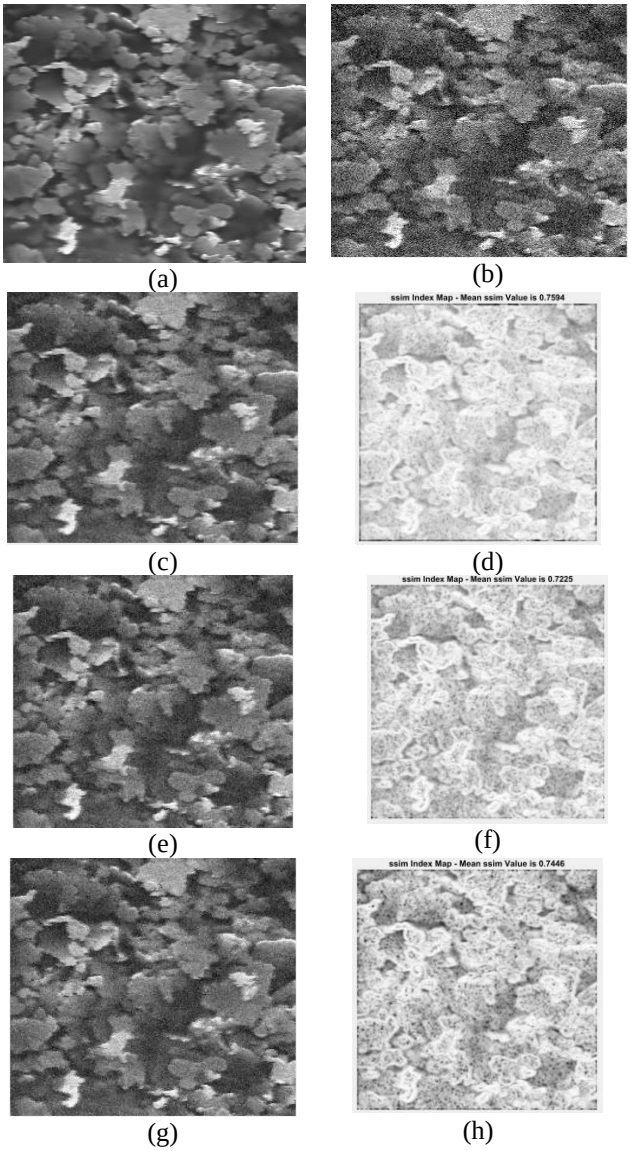

Fig. 30. (a) Original Material image A, (b) Corrupted Material image A with noise, (c) Average filtered image, (d) The SSIM index map of (c), (e) Median filtered image, (f) The SSIM index map of (e), and (g) Wiener (CSILLSR) filtered image and (h) The SSIM index map of (g).

TABLE XIII
MSE OF MATERIAL IMAGE A

Noise Variance	Average filter (MSE)	Median filter (MSE)	**Wiener filter (MSE)**
0.001	0.000355	0.000267	**0.000205**
0.002	0.000469	0.000445	**0.000373**
0.003	0.000574	0.000610	**0.000549**

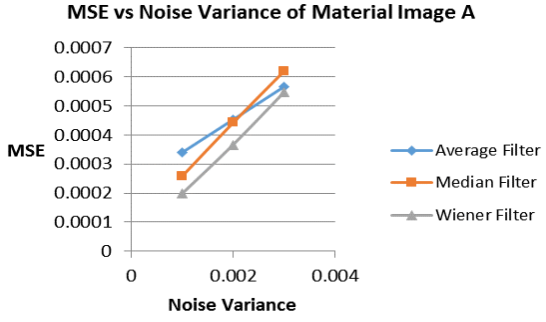

Fig. 31. Graph of MSE for three types of filters vs Noise Variance for Material Image A in Fig. 30

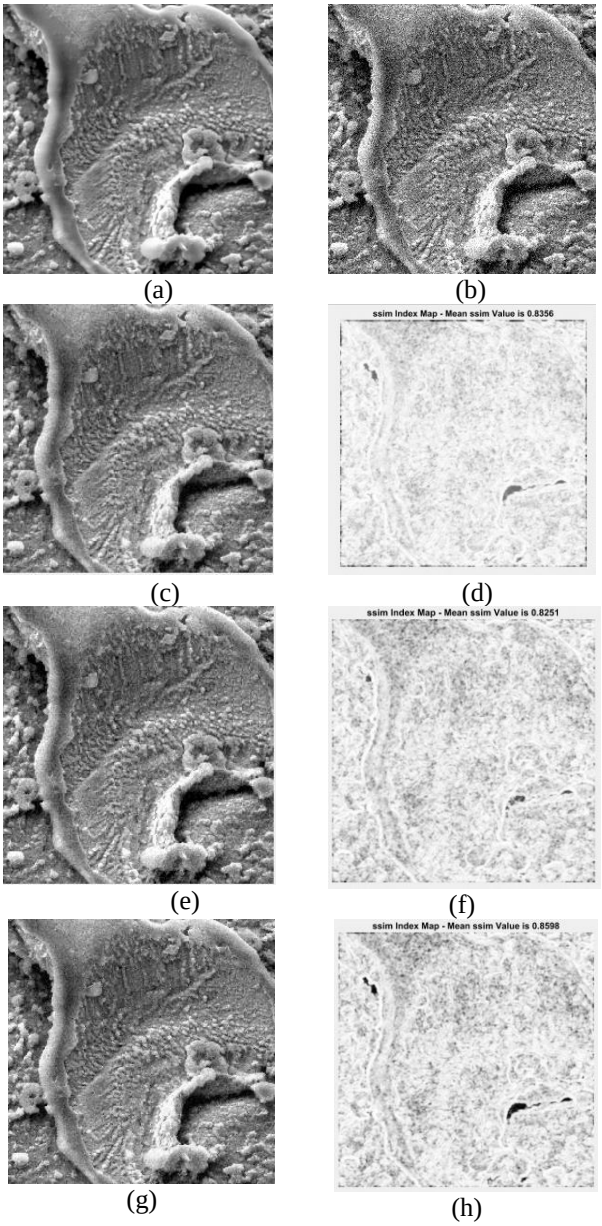

Fig. 32. (a) Original Material image B, (b) Corrupted Material image B with noise, (c) Average filtered image, (d) The SSIM index map of (c), (e) Median filtered image, (f) The SSIM index map of (e), and (g) Wiener (CSILLSR) filtered image and (h) The SSIM index map of (g).

TABLE XIV
MSE OF MATERIAL IMAGE B

Noise Variance	Average filter (MSE)	Median filter (MSE)	**Wiener filter (MSE)**
0.001	0.001355	0.001057	**0.000789**
0.002	0.001474	0.001284	**0.000967**
0.003	0.001589	0.001482	**0.001138**

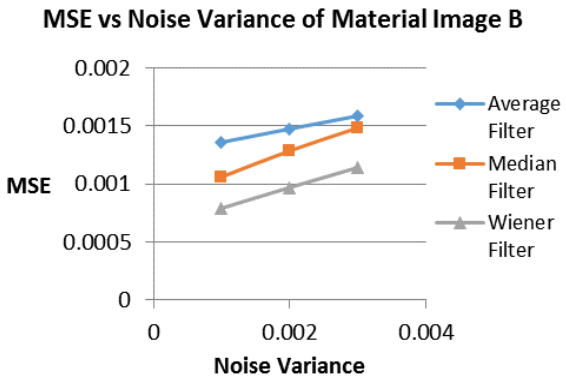

Fig. 33. Graph of MSE for three types of filters vs Noise Variance for Material Image B in Fig. 32.

The performances of Cubic Spline Interpolation with Linear Least Square Regression Wiener filter, Average filter and Median filter are compared in terms of the Mean Square Error (MSE) with four images. The results of the MSE of these four images for three types of filters are tabulated in Table XI to Table XIV. By referring to Table XI to Table XIV, the value of MSE increases as the noise variance increases. The quality of image is reduced when the amount of noise is high. Thus, lower image quality will result in higher MSE value.

According to the result in Table XI, the MSE for Wiener filter of IC compound A is at 0.000566 when the noise variance is given by 0.003, which is the lowest MSE value as compared with the other two filters. Similarly, the MSE result of the Wiener filter remains the lowest for Table XII, Table XIII and Table XIV of IC compound B, Material image A and Material image B, which are calculated at 0.000549, 0.000548 and 0.001138 respectively, while the noise variance is given by 0.003. Since the CSILLSR method managed to provide good accuracy of SNR value estimation for the SEM images, this justifies the result of lesser MSE value for Wiener filter that combined with CSILLSR method.

According to Figures 27, 29, 31, and 33, the Wiener filter has the highest performance compared to Average filter and Median filter. It appears that Wiener filter is the best filter to reduce and remove the white Gaussian noise from the SEM images as compared to the other two filters. Average filter gives the worst performance followed by Median filter. According to the results, it is clear that Median filter and Average filter are not suitable to filter out and reduce the white Gaussian noise from the scanning electron microscope images. Denoise process is proved to enhance image quality and provides more detail information. Several reviewed studies enhanced images through state-of-the-art methods [16][17][18].

IX. CONCLUDING REMARK

The present work shows that the cubic spline interpolation with linear least square regression yields the lowest absolute error difference, when compared with those obtained by other methods. CSILLSR provides the highest accuracy with acceptable stability when performing SNR estimation. When the noise variance rises from 0.001 to 0.010, CSILLSR estimation method tends to follow and estimate SNR value along the pattern of the ACF curve, thus giving high stability.

The present study also compares that increasing accelerating voltages and beam diameter will increase the image contrast. Increasing the surface tilt increases the ACF value. The combination of Wiener filter and CSILLSR method provides relatively low MSE value as compared with both Average and Median filters.

REFERENCES

[1] Z. X. Yeap; K. S. Sim and C. P. Tso, "Signal-to-noise ratio estimation technique for SEM image using B-spline,", the 2016 International Conference on Robotics, Automation and Sciences (ICORAS), pp. 1 - 5, DOI: 10.1109/ICORAS.2016.7872617, 2016.

[2] J. Frank and L. Al-Ali, "Signal-to-noise ratio of electron micrographs obtained by cross correlation,", *Nature*, vol 256, no. 5516, pp. 376-379, 1975

[3] S. J. Erasmus, "Reduction of noise in TV rate electron microscope images by digital filtering," *Journal of Microscopy* vol. 127, pp. 29-37, 1982.

[4] D. C. Joy, Y. U. Ko and J. J. Hwu, "Metrics of resolution and performance for CD-SEMs in metrology inspection and process control for microlithography," XIV. Proc SPIE, 3998, pp. 108-115, 2000.

[5] J. T. L. Thong, K. S. Sim, and J. C. H. Phang, "Single-Image Signal to Noise Ratio Estimation," *Scanning* , vol. 23, pp. 328-336, 2001.

[6] K. S. Sim, (2002), "Estimation of signal-to-noise ratio from single SEM image", Master thesis, National University of Singapore, 2002.

[7] K. S. Sim and S. K. Nidal, "Image signal-to-noise ratio estimation using autoregressive model,"*Scanning* vol. 26, pp. 135-139, 2004.

[8] K. S. Sim, H. T. Chuah, and C. Zheng, "Performance of a mixed Lagrange time delay estimation autoregressive (MLTDEAR) model for single-image signal-to-noise ratio estimation in scanning electron microscopy." *Journal of Microscopy,* vol. 219, no. 1, pp. 1-17, 2005.

[9] K. S. Sim, M. Y. Wee, and W. K. Lim, "Image signal-to-noise ratio estimation using shape-preserving piecewise cubic Hermite autoregressive moving average model," *Microsc.Res.Tech*. vol. 71, no. 10, pp.710-720, 2008.

[10] K. S. Sim and V. Teh, "Image signal-to-noise ratio estimation using adaptive slope nearest-neighbourhood model," *J. Microscopy*, vol. 260, no. 3, pp. 352– 362, 2015.

[11] K.S. Sim, Z.X. Yeap, C.P. Tso, "Signal-to-noise ratio estimation using adaptive tuning on the piecewise cubic Hermite interpolation model for images," Scanning vol. 38, no. 6, pp. 502–514, 2016.

[12] K. S. Sim, M. S. Lim and Z. X. Yeap, "Performance of signal-to-noise ratio estimation for scanning electron microscope using autocorrelation Levinson-Durbin recursion model," *Journal of Microscopy* vol. *00,* pp. 1-14. 2015.

[13] K. S. Sim and N. Syafiq, "Nonlinear least squares regression for single image scanning electron microscope signal-to-noise ratio estimation," *Journal of Microscopy*, vol. 264, no. 2, pp.159–174, 2016.

[14] T. Young and M. J. Mohlenkamp, "Introduction to Numerical Methods and Matlab Programming for Engineers," Methods, pp. 68–71, 2011.

[15] K. S. Sim, M. E. Nia, C. P. Tso, and W. K. Lim, " Performance of new signal-to-noise ratio estimation for SEM images based on single image noise cross-correlation," Journal of Microscopy, 248, pp. 120-128, 2012.

[16] F. F. Ting, K. S. Sim and E. K. Wong, "A rapid medical image noise variance estimation method," 2016 International Conference on Robotics, Automation and Sciences (ICORAS), Melaka, 2016, pp. 1-6. doi: 10.1109/ICORAS.2016.7872628

[17] C. P. Li, and H. B. Hao, "Degradation Data Analysis Using Wiener Process and MCMC Approach," Engineering Letters, vol. 25, no. 3, pp234-238, 2017.

[18] Z. Wang, B. Chen, J. Wu, and T. Yan, "Real-Time Image Tracking with An Adaptive Complementary Filter," IAENG International Journal of Computer Science, vol. 45, no.1, pp 228-234, 2018.

K. S. Sim received his Ph.D. degree from the Faculty of Engineering and Technology, Multimedia University, Malaysia, in 2005. He is now a full professor at Multimedia University. His research areas are signal and image processing, noise quantization, image color coding, biomedical imaging and biomedical engineering.

J. W. Leong received his B.Eng degree from the Faculty of Engineering and Technology, Multimedia University, in 2017.

F. F. Ting received her M.Eng.Sc degree from the Faculty of Engineering and Technology, Multimedia University in 2017. Currently, she is working as a researcher while pursuing her PhD degree in Multimedia University.

C. P. Tso received his Ph.D. from University of California, Berkeley in 1979. He is presently a professor at Multimedia University, Malaysia.